

**The impact of NO_x addition on the ignition behavior of *n*-pentane**

Journal:	<i>Reaction Chemistry & Engineering</i>
Manuscript ID	RE-ART-02-2021-000055.R1
Article Type:	Paper
Date Submitted by the Author:	11-Jul-2021
Complete List of Authors:	Fuller, Mark; RWTH Aachen University, Physico-Chemical Fundamentals of Combustion; Technion Israel Institute of Technology Morsch, Philipp; RWTH Aachen University, Physico-Chemical Fundamentals of Combustion Preußker, Matthias; RWTH Aachen University, Physico-Chemical Fundamentals of Combustion Goldsmith, C.; Brown University School of Engineering Heufer, K.; RWTH Aachen University, Physico-Chemical Fundamentals of Combustion

Cite this: DOI: 00.0000/xxxxxxxxxx

The impact of NO_x addition on the ignition behaviour of *n*-pentane[†]

Mark E. Fuller^{*a‡}, Philipp Morsch^a, Matthias Preußker^a, C. Franklin Goldsmith^b, and K. Alexander Heufer^aReceived Date
Accepted Date

DOI: 00.0000/xxxxxxxxxx

Modern engines concepts present several opportunities for nitrogen combustion chemistry, particularly the interaction of NO_x (NO + NO₂) with fuel fragments and products of partial combustion. Current mass-production internal combustion engines are routinely fitted with exhaust gas recirculation (EGR) systems which mix exhaust gases containing NO_x with the fresh charge of unburnt fuel and air. Further, interest in application of alkyl nitrates as reactivity enhancers in experimental engine concepts also leads to conditions in which the concentrations of NO_x and fuel or fuel fragments are high and the ensuing chemistry plays a major role in the mixture reactivity. In this work, ignition delay times for *n*-pentane doped with NO_x (NO + NO₂) were examined in a rapid compression machine. Blends of *n*-pentane and oxygen at stoichiometric ratios of 0.5, 1.0, and 2.0 were prepared in nitrogen or 1:1 nitrogen/argon bath gas blends at dilution ratios of 7.52:1 diluent:oxygen and doped with either NO or NO₂ at concentrations up to 1000 ppm. Ignition delay times were observed for post-compression pressures of 15 bar nominal and temperatures between 650 and 1000 K. A new chemical kinetic model is presented which is constructed upon recent, verified literature mechanisms for pentane combustion and for the combustion of small hydrocarbons and nitrogenated species. Additional recent developments in nitrogen combustion chemistry are applied to update the mechanism and new classes of reactions between fuel fragments and nitrogenated species are introduced and added systematically to the model. The reaction rates for the mechanism are taken from literature or estimated by analogy and are then manually adjusted as informed by simulation results and sensitivity analysis. Further fine optimization of the model is accomplished utilizing an automated routine. Comparison is made to another pentane-NO_x model in literature and the associated data from jet-stirred reactor (JSR) experiments. The model presented in this work is found to have superior performance in predicting and modeling the ignition delay times and similar behaviour in reproducing the JSR species profiles as compared with the baseline literature mechanism.

1 Introduction

Development and refinement of combustion chemistry which includes detailed reactions with nitrogen oxides (NO_x) and hydrocarbons is an active topic of research^{1–5}. Current mass-production internal combustion engines are routinely fitted with exhaust gas recirculation (EGR) systems to control and reduce

undesirable exhaust products, including NO_x^{4,6}. However, the recirculation of exhaust gases into the engine cylinder and mixture with the fresh charge of unburnt fuel and air presents opportunities for chemical reactions between the combustion reactants and products in concentrations and conditions that merit additional study⁴. Further, the interest in application of alkyl nitrates as reactivity enhancers in experimental engine concepts^{5,7–9} also leads to conditions in which the concentrations of NO_x and fuel or fuel fragments are high and the ensuing chemistry plays a major role in the in the mixture reactivity. Motivating experimental studies include flow reactor studies of C₂H₄/O₂/NO mixtures under high pressure (60 bar) and temperatures of 600 K to 900 K¹⁰: the experiments found significant removal of NO_x which was not predicted by the kinetic mechanism, suggesting that current mod-

^a Physico-Chemical Fundamentals of Combustion, RWTH Aachen University, 52062 Aachen Germany; E-mail: fuller@pcfc.rwth-aachen.de

^b School of Engineering, Brown University, Providence, RI 02912, USA

[†] Electronic Supplementary Information (ESI) available: enlarged versions of and additional figures, chemical kinetic mechanisms, and experimental data. See DOI: 10.26434/chemrxiv.13720105 (temporary preprint DOI)

[‡] Present address: Faculty of Chemical Engineering, Technion I.I.T., Haifa 3200003, Israel

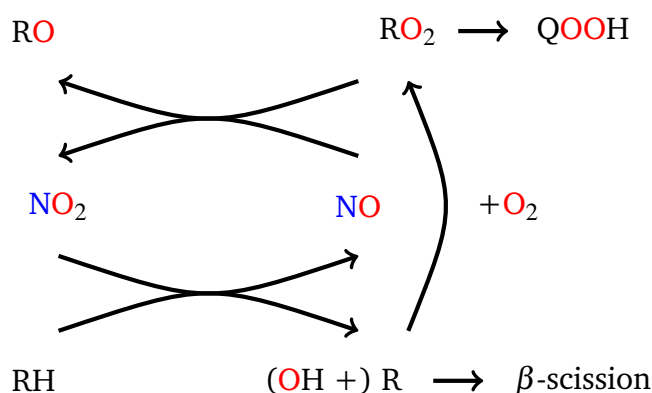


Fig. 1 Key pathways in NO_x cycling

els do not accurately capture low-temperature nitrogen chemistry and fuel- NO_x interactions. When examining alkyl nitrates, specifically 2-ethylhexyl nitrate (EHN), in low-temperature compression ignition (LTCI) engines, model predictions and experimental measures also diverge: roughly one-third of the fuel-bound nitrogen was measured experimentally in the exhaust as NO_x ^{11–13} with the remaining nitrogen unaccounted for, *i.e.* not detected using the experimental methods in the study.

Regardless of the source, the presence of NO_x has an ignition-promoting (reactivity-enhancing) effect^{1–3}: NO_2 serves to promote chain-branching by abstracting a hydrogen to form HONO or HNO_2 , both of which may then decompose to OH and NO ¹⁴. NO may recycle to NO_2 particularly through interactions with peroxy radicals, as depicted in figure 1.

A number of recent mechanisms are relevant to development of a detailed mechanism for combustion of *n*-pentane in the presence of NO_x . The mechanism of Bugler *et al.*¹⁵ for combustion of all three pentane isomers is extremely well validated across a range of experimental conditions. Mechanisms specific to the combustion of *n*-pentane in the presence of NO_x have been developed sequentially utilizing Bugler *et al.* as a base mechanism by Zhao *et al.*^{16,17} and Marrodán *et al.*, which included jet-stirred reactor (JSR) experiments of pentane doped with NO_x .

Further, more detailed nitrogen-combustion chemistry, extending beyond NO_x mechanisms, in the presence of small hydrocarbons is also an area of active development. As discussed in¹⁸, these mechanisms include those published by Dagaut *et al.*¹⁹ and Konnov²⁰, which do not include HNO_2 as a unique species. Mechanisms published by Abian *et al.*²¹, Ahmed *et al.*²², Glarborg *et al.*^{3,10,23}, Mathieu *et al.*^{24,25}, and Zhang *et al.*²⁶ do, however, contain HNO_2 .

Additionally, theoretical work has been recently published by Goldsmith and coworkers^{5,7,14,18,27,28} for a number of subsystems relevant to nitrogen combustion chemistry, including the HNO_2 potential energy surface¹⁴, fuel + NO_2 hydrogen abstractions²⁷ and associated potential energy surfaces¹⁸, $\text{R} + \text{NO}_2$ ²⁸, and combined experimental and theoretical investigation of isopropyl nitrate^{5,7}.

2 Experimental

Experiments were conducted in the rapid compression machine (RCM) facility in the Physico-Chemical Fundamentals of Combustion research group at RWTH Aachen University. The facility has been described in detail elsewhere²⁹ and details of the theory and application of RCMs in chemical kinetics are covered in detail by Sung and Curran³⁰. Briefly, the apparatus utilizes a single piston which is pneumatically-driven and hydraulically-stopped. A movable endwall allows for compression ratios between 9 and 32 and a creviced piston minimizes vortex rollup during the compression stroke. The range of post-compression temperatures is further extended by varying the heat capacity of the diluent gas by utilizing nitrogen, argon, carbon dioxide and mixtures thereof. Simulation of experiments is conducted by repeating each experimental condition with a non-reactive experiment in which the oxygen is substituted for nitrogen, preserving the heat capacity of the mixture, in order to produce an effective volume profile. Effective volume profiles are utilized to simulate experiments while accounting for facility effects, such as heat loss, which is also described by Sung and Curran³⁰. Mixtures were prepared manometrically. All gases were supplied by Westfalen AG. Oxygen (purity 99.999%), nitrogen (purity 99.999%), and argon (purity 99.997%) were utilized as neat gas sources. For NO_x , mixtures of 2% NO and 1% NO_2 (purity 99%) in N_2 (purity 99.999%) were purchased from Westfalen AG., *n*-Pentane (purity 99.4%) was purchased from VWR. Detailed experimental data are provided as supplementary material[†].

3 Kinetic Model

In this work, we present the results of RCM measurements of ignition delay times (IDTs) for blends of *n*-pentane doped NO_x and a new chemical kinetic model. The model presented here utilizes these most recent experimental data to inform a number of fitting parameters, but it also intended to be a first step in developing a full CHON mechanism for larger hydrocarbon fuels, representative of liquid fuels used in commercial and consumer applications.

The model builds on the well-validated mechanism of Bugler *et al.*¹⁵ for pentane combustion. Relevant pathways and classes of reactions between *n*-pentane and NO_x are drawn from the recent work of Marrodán *et al.*⁴, which included jet-stirred reactor (JSR) experiments of pentane doped with NO_x .

Significant updates are made to the proposals of Marrodán *et al.*, most prominently the inclusion of the full nitrogen combustion mechanism of Glarborg *et al.*³ and the accompanying thermodynamic data from the Active Thermochemical Tables (ATcT)^{31–33}, especially the treatment of HNO_2 as a unique species from HONO ¹⁸ and utilizing the latest high-level calculations of Goldsmith and coworkers^{5,7,14,18,27,28}.

As also discussed in¹⁸, there are a number of mechanisms for small hydrocarbons and NO_x which have been utilized in recent publications. As mentioned above, based on that work, it is believed proper to include HNO_2 as a unique species from HONO , which is not the case in the mechanism of Marrodán *et al.*

Kinetic simulations were performed in CANTERA³⁴ using an

in-house toolkit for simulation of RCM experiments from non-reactive volume profiles³⁰.

Mechanism development proceeded from systematic addition of classes of potential reactions in order to consider the full parameter space of potential reactions before performing sensitivity analyses and optimizing the model.

Several revisions were made to the mechanism of Glarborg *et al.*:

- The HNO₂ potential energy surface (PES) reactions calculated by Chen *et al.*¹⁴
- Rate constants for the H₂NO₂ and CH₄NO₂ PES from Fuller and Goldsmith¹⁸
- Hydrogen abstraction by NO₂ from alkanes and alkenes as published by Chai and Goldsmith²⁷ and refit to the exothermic direction^{7,18}
- Decomposition rates for nitromethane (and related reactions)³⁵, alkyl nitrites³⁶, and isopropyl nitrate⁵
- The C₃H₃NO PES as calculated by Danilack and Goldsmith²⁸

Initial values of rate constants for new reactions were estimated, where possible, by analogy to known values for similar reactions. In this project, the Reaction Mechanism Generator (RMG)^{37,38} was utilized to estimate rate constants for new classes or reactions for which analogies were not available. Further, thermodynamic data for new species was computed using RMG and group additivity methods³⁹. Additional *ab initio* calculations of rate constants were performed drawing on previous work for interactions between NO₂ and hydrocarbons^{18,27}. Geometry optimization and normal mode analysis were performed using the B2PLYPD3 functional with the cc-pVTZ basis set^{40–42} using GAUSSIAN16⁴³. Additional single-point calculations were carried out on the optimized geometries at the DLPNO-CCSD(T)-F12/cc-pVTZ-F12 level⁴⁴, run in ORCA⁴⁵. Calculations executed in ORCA utilized the auxiliary basis sets cc-pVTZ/C and cc-pVTZ-F12-CABS and the TightSCF option. For elementary reactions with tight transition states, transition state theory (TST) calculations were performed with the TAMKIN code⁴⁶. Additional master equation calculations for pressure-dependent kinetics utilized the RRKM/ME code MESS^{47,48}, which is part of the computational kinetics package PAPR⁴⁹. Specific calculations are described in detail, below.

3.1 Hydrogen abstractions by NO_x

Following on the recommendations presented in Fuller and Goldsmith¹⁸ regarding the proper inclusion of HNO₂ as a unique species, hydrogen abstraction reactions by NO₂ to form HNO₂ were added in cases where only a reaction to HONO was present in the mechanism of Glarborg *et al.* The added reactions are listed in table 1. Rate constants for which the reference is the present work (P.W.) were calculated as described above at the DLPNO-CCSD(T)-F12/cc-pVTZ-F12//B2PLYPD3/cc-pVTZ level of theory

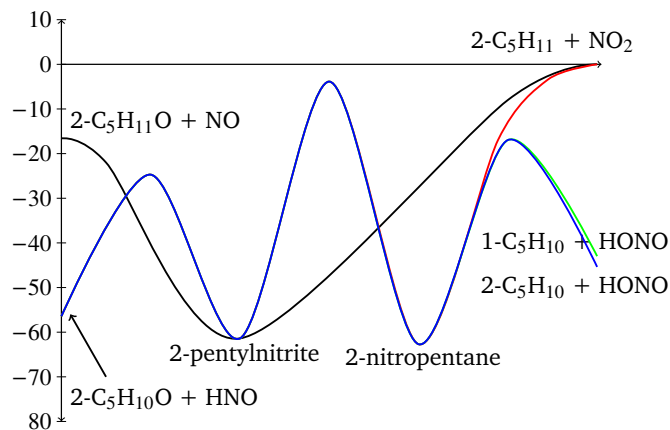


Fig. 2 Potential energy surface for the 2-pentyl + NO₂ system. Energies in kcal/mol.

and with TAMKIN. Reactions are written in the exothermic direction in order to minimize error associated with revisions to thermodynamic data¹⁸. Other cursory estimates were made either utilizing the RMG rate rules³⁸ or by analogy to the work of Chai and Goldsmith²⁷.

Further additions to the mechanism were made as classes of reactions. Hydrogen abstraction by NO₂ from *n*-pentane to form the three *n*-pentyl radicals and both HONO and HNO₂ (six reactions) were added by analogy with the rate constants for abstraction from *n*-butane in Chai and Goldsmith²⁷.

Hydrogen abstraction from closed-shell species by NO was also considered. Utilizing the same theoretical methods, the hydrogen abstraction from propane by NO to form both *n*-propyl and *i*-propyl were calculated. These results were applied by analogy to estimate rate constants for abstractions from ethane, *n*-butane, and *n*-pentane with the rate to form *n*-propyl assigned for abstractions from primary carbons and for *i*-propyl to secondary carbons.

Further hydrogen abstractions by NO_x from alkyl radicals to form alkenes were also added to the model. All abstractions by NO to form HNO and an alkene were added using rate constants suggested by RMG. For abstractions by NO₂, reactions with ethyl, *n*-propyl, *i*-propyl, 1-butyl, and 2-butyl radicals forming HONO were also taken from RMG rate rules. A full PES for 2-pentyl and NO₂ (see figure 2) was calculated and rate constants for 1-pentyl and 3-pentyl were included as analogies to the 2-pentyl rate.

Rate constants involving 1-pentyl were assumed as equivalent to those for 2-pentyl. For 3-pentyl, the pre-exponential factors, *A* were assumed to be one-half those of the corresponding values for 2-pentyl based on the number of sites; the activation energies, *E_a*, and temperature exponents, *n*, are kept constant. The full details of the calculation of the 2-pentyl + NO₂ PES are part of a forthcoming manuscript on R + NO₂ kinetics.

The hydrogen abstraction reactions from alkenyl radicals by NO₂ to form a radical, an aldehyde, and NO were included for some species by Marrodán *et al.*⁴ and have been extended to all four and five carbon straight-chain alkenyl radicals by analogy.

Hydrogen abstractions from alkyloxy radicals to carbonyls (aldehydes and ketones) was similarly considered: The reaction of 2-pentylloxy and NO to 2-pentanone and HNO was determined

Table 1 $\text{RH} + \text{NO}_2 = \text{R} + \text{HNO}_2$ pathways added to the mechanism of Glarborg *et al.*³. Units: cal, mol, cm, s, K; $k = AT^n \exp(-E_a/RT)$.

Reaction	A	n	E_a	References
$\text{CH}_3\text{O} + \text{NO}_2 \rightleftharpoons \text{CH}_2\text{O} + \text{HNO}_2$	5.16e+02	2.96	4690	P.W.
$\text{CH}_2\text{CHO} + \text{NO}_2 \rightleftharpoons \text{CH}_2\text{CO} + \text{HNO}_2$	3.03e+02	2.99	32050	P.W.
$\text{NH}_2 + \text{HNO}_2 \rightleftharpoons \text{NH}_3 + \text{NO}_2$	9.10e+05	1.94	-1150	RMG-Py rate rules ³⁷
$\text{NH} + \text{HNO}_2 \rightleftharpoons \text{NH}_2 + \text{NO}_2$	2.65e+08	1.50	-350	RMG-Py rate rules ³⁷
$\text{H}_2\text{NO} + \text{NO}_2 \rightleftharpoons \text{HNO} + \text{HNO}_2$	1.10e+04	2.64	4040	Est. 1/4 HONO rate ³
$\text{HNOH} + \text{NO}_2 \rightleftharpoons \text{HNO} + \text{HNO}_2$	1.50e+11	0.00	2000	Est. 1/4 HONO rate ³
$\text{CN} + \text{HNO}_2 \rightleftharpoons \text{HCN} + \text{NO}_2$	4.20e+06	1.91	-510	RMG-Py rate rules ³⁷
$\text{NCO} + \text{HNO}_2 \rightleftharpoons \text{HNCO} + \text{NO}_2$	1.13e+05	2.31	-1380	RMG-Py rate rules ³⁷
$\text{CH}_2\text{OH} + \text{NO}_2 \rightleftharpoons \text{CH}_2\text{O} + \text{HNO}_2$	1.25e+12	0.00	0	Est. 1/4 HONO rate ⁵⁰
$\text{C}_2\text{H}_5\text{O} + \text{NO}_2 \rightleftharpoons \text{CH}_3\text{CHO} + \text{HNO}_2$	4.00e+11	0.00	0	Est. 1/4 HONO rate ^{51,52}
$\text{CH}_2\text{NO}_2 + \text{HNO}_2 \rightleftharpoons \text{CH}_3\text{NO}_2 + \text{NO}_2$	1.66e+12	-0.05	1020	RMG-Py rate rules ³⁷

from the aforementioned PES. The rate constants for 1-pentyloxy and 3-pentyloxy were, again, derived by analogy to 2-pentyloxy. For all other abstractions by NO, analogies were drawn to the rate of Daële *et al.*⁵³ for $\text{C}_2\text{H}_5\text{O} + \text{NO} \rightleftharpoons \text{CH}_3\text{CHO} + \text{HNO}$.

Abstractions by NO_2 to form HONO were analogized to the rate for $\text{C}_2\text{H}_5\text{O} + \text{NO}_2 \rightleftharpoons \text{CH}_3\text{CHO} + \text{HONO}$ included in Glarborg *et al.*^{3,51,52}. Corresponding rate constants to form HNO_2 were again estimated from the rate to form HONO.

3.2 Unimolecular conformer formation and dissociation

Recombination of NO_x and another radical to a unimolecular conformer and the corresponding dissociation rate were also added as classes of reactions, drawing largely again on the work of Glarborg *et al.* and Marrodán *et al.*

The formation of nitro compounds from alkyl radicals and NO_2 was taken from Marrodán *et al.*⁴ for *n*-propyl, *i*-propyl, 1-butyl, and 2-butyl. For 2-pentyl, the rate was taken from our PES results and rate constants for 1-pentyl and 3-pentyl were added by analogy.

For nitrite species formed from alkyl radicals and NO_2 , rate constants for C_1 through C_4 radicals were estimated using RMG rate rules³⁷. The rate for 2-pentyl was again taken our calculated results and rate constants for 1-pentyl and 3-pentyl were added by analogy.

All reactions of alkyl radicals and NO to form nitroso compounds were estimated with RMG rate rules³⁷. Nitroso compounds resulting from NO attacking an olefinic bond were not explicitly considered or added to the model, but should be considered in future developments.

For nitrite and nitrate compounds reacting to and from an alkyloxy radical and NO or NO_2 , respectively, rate constants for *n*-propyl nitrite, *n*-butyl nitrite, and *i*-butyl nitrite were taken from the work of Randazzo *et al.*³⁶. The rate for 2-pentyl nitrite was again taken our calculated results and rate constants for 1-pentyl nitrite and 3-pentyl nitrite were added by analogy. The rate for *n*-propyl nitrate was taken from Mendenhall *et al.*⁵⁴ and extended by analogy to 1-butyl nitrate and 1-pentyl nitrate. The rate for *i*-propyl nitrate was taken from Fuller and Goldsmith⁵ and rate constants for 2-butyl nitrate, 2-pentyl nitrate, and 3-pentyl nitrate were all taken by analogy to this rate.

Recombination of alkyloxy and peroxy radicals (RO and RO_2) with NO_2 and NO, respectively, to form ROONO was added for

all *n*-alkyl radicals as a class of unimolecular sinks to NO_x cycling reactions (see below). Estimated rate constants were taken from RMG.

Additionally, formation reactions for ROONO_2 from a peroxy radical and NO_2 were added for the three pentyl radicals with estimates from RMG.

3.3 Isomerizations

Rate constants for the isomerization of nitro to nitrite compounds were also included for each of the three pentyl conformers. Isomerization of 2-pentyl nitrite to 2-nitropentane was taken our calculated results and rate constants for 1-pentyl and 3-pentyl were added by analogy.

3.4 Concerted HONO elimination

As a corollary to formation and dissociation of unimolecular compounds via the creation or breaking of a single bond, concerted HONO elimination reactions were also added to the model. Based on the findings for *i*-propyl nitrate by Fuller and Goldsmith⁵, these are not expected to play a significant role, but are included for completeness. Concerted elimination from both 2-nitropentane and 2-pentyl nitrite was included in the aforementioned calculation for the 2-pentyl + NO_2 PES, with rate constants developed by analogy for the corresponding 1-pentyl and 3-pentyl conformers.

3.5 NO_x cycling reactions

Besides hydrogen abstractions by NO_x , the other reaction class of major importance to NO_x combustion chemistry is NO_x cycling where NO and NO_2 interconvert¹⁶. Disproportionations between an alkyl radical and NO_2 on one side and an alkyloxy radical and NO on the other were taken from Rissanen *et al.*⁵⁵ for *n*-propyl, *i*-propyl, and 2-butyl with the rate for 1-butyl assumed by analogy with *n*-propyl. The rate for 2-pentyl was included in our master equation and 1-pentyl and 3-pentyl were taken by analogy with this rate.

For reactions where a peroxy radical and NO disproportionate to an alkyloxy radical and NO_2 , the reactions including ethyloxy, *n*-propyloxy, and *i*-propyloxy were taken from Atkinson *et al.*⁵⁶ and extended to the butyloxy and pentyloxy conformers by analogy. The reaction $\text{HNO} + \text{NO}_2 \rightleftharpoons \text{HNO}_2 + \text{NO}$ is also added to

this category and taken from the work of Marrodán *et al.*⁴.

3.6 Additional reactions

All other reactions involving nitrogen from the mechanism of Marrodán *et al.* are preserved in the present work, except for attack of post-second-oxygen-addition species of the structure OOQOOH, Q = C₅H₁₀, by NO to dissociate to OH + 2CH₂O + C₃H₆ + NO₂. These reactions were found to have minimal impact on predicted IDTs. The non-elementary nature make them poor candidates for systematic expansion of the mechanism. Comparison of the mechanism performance with and without these reactions is made. Further investigation into these low-temperature pathways and their analogues is not made at this time, but is planned to feature in future work.

Reactions between NO₂ and an aldehyde to products R + CO + HONO for ethanal (acetaldehyde) / methyl, propanal / ethyl, butanal / *n*-propyl, and isobutanal / *i*-propyl were present in the mechanism of Marrodán *et al.* By analogy, this class was extended to include pentanal / 1-butyl and 2-methylbutanal / 2-butyl. Further, to all of the preceding reactions, the corresponding reaction to form HNO₂ was added with the rate estimated as one-quarter of the rate to form HONO, based on the work of Chai and Goldsmith which found that for C₀ to C₄ alkanes the branching fractions to HNO₂ ranged from approximately 10% to 40%.

The HNO₃ submechanism of Mueller *et al.*⁵⁷ has also been mechanistically retained by way of inclusion of HO₂ + NO + M ⇌ HONO₂ + M and NO + HO₂ ⇌ O₂ + HONO₂.

4 Results and Discussion

4.1 RCM

As in Marrodán *et al.*⁴, the pentane mechanism of Bugler *et al.*¹⁵ was utilized as a starting point in the present study. For validation purposes, neat *n*-pentane ignition delay experiments were conducted and compared to the mechanisms of Bugler *et al.* and Marrodán *et al.* alongside the mechanism of the present work (figure 3). No detailed analysis of the mechanism of Marrodán *et al.* has been performed to understand the loss in fidelity for predictions of *n*-pentane ignition with respect to the mechanism of Bugler *et al.* (on which both Marrodán *et al.* and the present work are based).

The mechanism presented here, however, reproduces the predictions of Bugler *et al.* Further, it includes all mechanistic pathways regarding the interaction of NO_x with *n*-pentane included in Marrodán *et al.* and adds additional reactions and classes which may be generally important for CHON chemistry.

Comparison of experiments at stoichiometric conditions for neat *n*-pentane and with different initial dopants (333 ppm NO₂ and 1000 ppm NO) are depicted in figure 4. For both dopants, the influence on ignition delay times is minor at the lowest temperatures and accordingly the low-temperature branch, but becomes significant at high temperatures.

For both doping cases, a reactivity increasing-effect is observed which is higher for the case of an initial doping of 1000 ppm NO. During the post-processing of the data, kinetic simulations suggested an almost complete conversion of NO to NO₂ by reaction

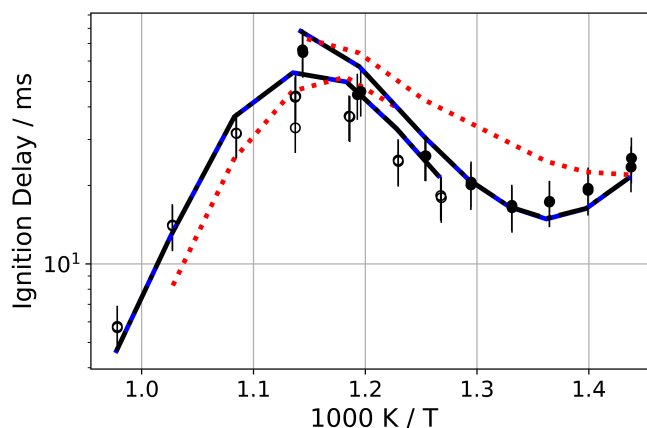


Fig. 3 Comparison of model predictions for neat, stoichiometric *n*-pentane ignition delay times; $P_c=15$ bar, mixtures in synthetic air diluted with additional nitrogen or argon as indicated. $n\text{-C}_5\text{H}_{12} : 8 (\text{O}_2 + 3.76 \text{N}_2 + 3.76 \text{X})$ where X is either N₂ or Ar. Closed symbols (●) are experiments conducted with N₂ diluent; open symbols (○) are Ar diluent. The solid blue line (—) is the model presented in this work. The black dash-dot line (— · — ·) is that of the pentane isomers model of Bugler *et al.* The red dotted line (· · · · ·) is the model of Marrodán *et al.*

of NO with O₂, already in the mixing vessel within 30 minutes. To confirm this theoretical analysis, gas mixtures with initial NO doping and typical experimental condition ($T = 75$ °C, $p = 5$ bar) have been analyzed immediately after mixture preparation using Fourier-transform infrared (FTIR) spectroscopy. Even after the relatively short time needed for mixture preparation and mixture analysis, in the order of a couple of minutes, high conversion rates of NO to NO₂ of more than 80 % were measured. This leads to the conclusion that for the initially NO doped mixtures a full conversion of the NO to NO₂ can be expected. A final cross-check was performed by performing experiments with 1000 ppm NO and 1000 ppm NO₂ initial doping against neat *n*-pentane in a second RCM. This RCM works analogous to the already discussed one but has slightly different compression characteristics leading to somewhat shorter measured ignition delay times. The repetition of the data in this machine confirmed the trends already visible in figure 4 (see suppl. Material Fig. S10). Furthermore, the differences between the initial NO or NO₂ doping are within the expected experimental uncertainty and therefore confirm the assumption of a complete conversion of NO to NO₂. For this reason, all experiments with an initial NO doping are treated as experiments with an equivalent NO₂ doping in simulation and analysis in the following. To conclude, even after short mixing times as it has been used in a previous studies⁵⁸ significant conversion of NO to NO₂ might be expected and conventional pre-mixing does not seem to be easily applicable for RCM or even shock tube experiments in the case of NO doping.

After assembling the mechanism, as described above, initial simulations and sensitivity analysis were used to make coarse, manual changes to improve the fit before executing an optimization routine on selected reactions. As originally implemented, the mechanism badly over-predicted ignition delay times (IDTs), especially in the low-temperature region: RMG-based estimations

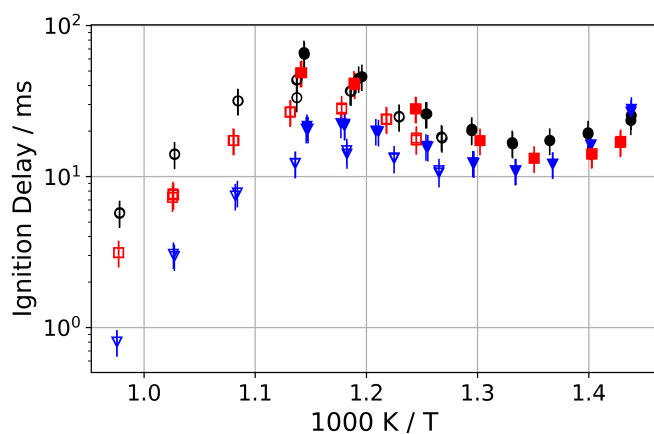


Fig. 4 Comparison of stoichiometric *n*-pentane ignition delay times; $P_C=15$ bar, mixtures in synthetic air diluted with additional nitrogen or argon as indicated. $n\text{-C}_5\text{H}_{12} : 8 (\text{O}_2 + 3.76 \text{N}_2 + 3.76 \text{X})$ where X is either N_2 or Ar. Closed symbols are experiments conducted with N_2 diluent; open symbols are Ar diluent. *n*-pentane, $\phi = 1.0$, neat (\bullet \circ), doped with 333 ppm NO_2 (\blacksquare \square) or 1000 ppm NO (\blacktriangledown \triangledown)

for hydrogen abstractions from alkyl radicals by NO_x were identified as most problematic and their reaction rates were reduced by a factor of one-hundred. This decision was made as these reactions, based on preliminary sensitivity analysis, appeared to be decisive in the excessively long IDTs observed in simulations and were based strictly on templates in RMG, not experimental measurements of theoretical computations. The " NO_x -cycling" reactions of the form $\text{R} + \text{NO}_2 \rightleftharpoons \text{RO} + \text{NO}$ and $\text{RO}_2 + \text{NO} \rightleftharpoons \text{RO} + \text{NO}_2$ were taken from or analogized to the work of Rissanen *et al.*⁵⁵ and Atkinson *et al.*⁵⁶, respectively, as described above. In both cases, the experimental data on which the rates are based is for significantly lower temperatures (below 500 K) and pressures (one bar and below). These rates constants, as published, were found to be much too fast in the range of the RCM experiments reported here and were refit to approximately match the rates and temperatures reported in literature and to be reduced by factors of ten and one-hundred, respectively, at the temperature range covered by the RCM experiments. The full chemical kinetic mechanism (v.0) included as supplemental material includes a changelog with sources, dates, and modifying factors. The inclusion of the rate modifications as variable multipliers allows for any user to easily undo our rate modifications or make further adjustments.

Other classes of reactions of NO_x and a radical to a unimolecular conformer were adjusted as well: Reactions of the form $\text{R} + \text{NO}_2 \rightleftharpoons \text{RONO}$, taken from RMG rate rules, were also reduced by a factor of ten, while those for $\text{RO}_2 + \text{NO}_x \rightleftharpoons \text{ROONO}_x$, also from RMG, were ultimately reduced by a factor of one thousand. Dissociation reactions $\text{RNO}_2 \rightleftharpoons \text{R} + \text{NO}_2$, taken from the work of Marrodán *et al.*, were increased by a factor of two. Further, the two dissociation reactions of nitromethane ($\text{CH}_3\text{NO}_2 \rightleftharpoons \text{CH}_3 + \text{NO}_2$, $\text{CH}_3\text{NO}_2 \rightleftharpoons \text{CH}_3\text{O} + \text{NO}$) are taken from the combined experimental and theoretical study of Annesley *et al.*³⁵.

For the above classes of reactions for which major reductions in the rates were made (factor of ten or greater), these are all

radical-radical reactions. In low-pressure systems, it may be that the disproportionation reactions ($\text{R} + \text{NO}_2$ H-abstraction, $\text{R} + \text{NO}_2 \rightleftharpoons \text{RO} + \text{NO}$, and $\text{RO}_2 + \text{NO} \rightleftharpoons \text{RO} + \text{NO}_2$) dominate, but for higher, engine-relevant pressures, stabilization of unimolecular intermediates and isomerization thereof may play an important role. For this reason, these classes of reactions, as described above, were added to the mechanism and filled out to include all relevant species. Our ability to estimate or guess at these phenomena is unfortunately currently limited, as evidenced by the major rate reductions required when adding pathways to the ROONO_x wells. Additional high-level calculations of the potential energy surfaces which the aforementioned radical-radical interactions are needed to replace the current Arrhenius fits with full pressure-dependent estimates, which may serve to bridge the divide between the present work and previous studies conducted near atmospheric pressure. A future computational study on these reactions is planned in order to elucidate and further develop these mechanistic pathways.

Further discussion of the process of adjusting classes of reactions rates and their impacts on model performance are provided in the supplementary materials.

The final sensitivities of the mechanism as developed to this point are depicted in figures 5 and 6, what shall be referred to as the "version zero" or "v.0" mechanism presented in this work. For sensitivity calculations, we have used the reanalyzed mixture composition where NO is fully converted to NO_2 in the case of mixtures prepared with NO as the dopant, i.e. sensitivity analysis is performed on mixtures doped with 333 and 1000 ppm NO_2 . Only the sensitivities for $\phi=1.0$ are included here; results for $\phi=0.5$ and $\phi=2.0$ are available in the supplemental materials. Sensitivities of individual reactions among those added to the mechanisms of Bugler *et al.* and Glarborg *et al.* are shown for temperatures from 650 K to 900 K in 50 K increments. Unsurprisingly, the most sensitive reactions for both doping conditions are largely the same. For NO_2 -doping, hydrogen abstraction by NO_2 is particularly sensitive, as one would expect, *c. f.* Chai and Goldsmith²⁷. Primary and secondary site hydrogen abstraction by NO_2 to form HONO has an ignition-promoting effect, which is least prominent in the NTC region, but grows as the temperature moves away from the NTC, with a significantly larger effect in the high-temperature branch. The HONO PES, calculated by Chen *et al.*¹⁴, also dominates the sensitivities as reactions of NO and OH to HONO, HNO_2 , and $\text{H} + \text{NO}_2$ are all present in the ten most sensitive reactions at both conditions and all of which are ignition-promoting for the forward direct as written into the mechanism. For these first five sensitive rates, they all original in the Goldsmith research group and purely theoretical studies. Of the remaining five of the top-ten reactions for both conditions, both include reactions of methyl and NO_2 to both methyl nitrite and nitromethane, with nitromethane dissociation having a strong ignition-retarding effect in the NTC region and formation of methyl nitrite leading to increased IDTs at all temperatures, but with stronger effect at increasing temperatures. The current rate for nitromethane is taken from the work of Annesley *et al.* is a combined experimental and theoretical study³⁵. Conversely, the rate of methyl nitrite formation is originally determined from

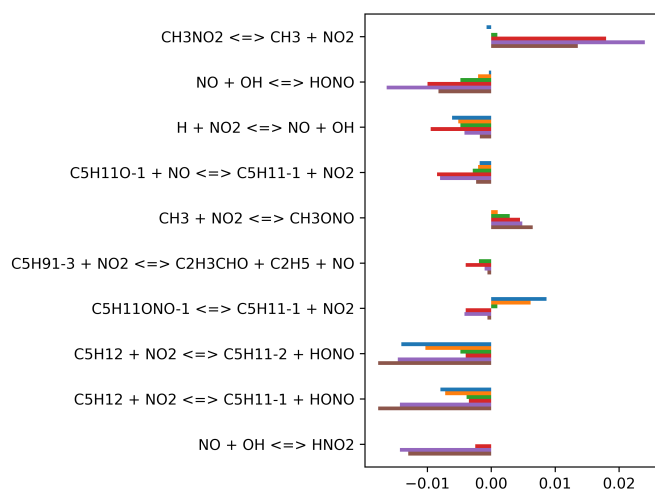


Fig. 5 Mechanism v.0: top sensitivities ($\frac{\partial \ln \tau}{\partial \ln k}$) among reactions added to the mechanisms of Bugler *et al.*¹⁵ and Glarborg *et al.*³ for *n*-pentane in synthetic air diluted with N₂ at equivalence ratios of $\phi = 1.0$ and with 333 ppm NO₂. Individual bands represent analysis at temperatures of 650 K (top, blue) to 900 K (bottom, brown) in 50 K increments.

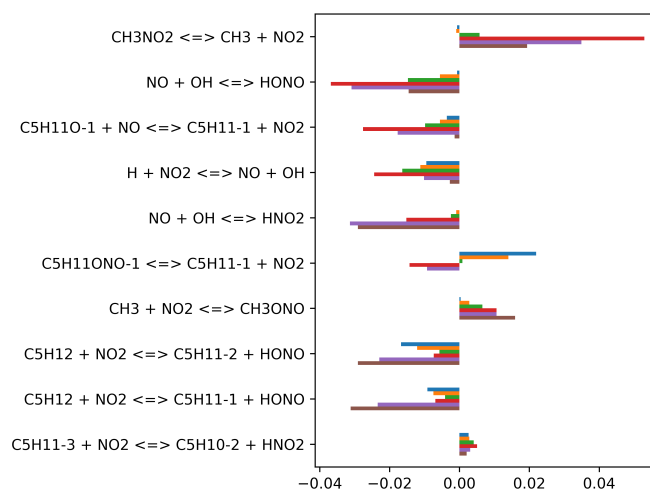


Fig. 6 Mechanism v.0: top sensitivities ($\frac{\partial \ln \tau}{\partial \ln k}$) among reactions added to the mechanisms of Bugler *et al.*¹⁵ and Glarborg *et al.*³ for *n*-pentane in synthetic air diluted with N₂ at equivalence ratio of $\phi = 1.0$ and with 1000 ppm NO₂. Individual bands represent analysis at temperatures of 650 K (top, blue) to 900 K (bottom, brown) in 50 K increments.

RMG rate rules and considered for optimization, below. The remaining three reactions from each set of conditions contain reactions about which there is uncertainty, including NO_x-cycling and nitrite dissociation to R + NO₂, both of which are derived from new quantum mechanical calculations conducted as part of this work. Additionally, there is hydrogen abstraction by NO₂ from a radical, derived by analogy from new quantum mechanical calculations, and finally a reaction from the mechanism of Marrodán *et al.*, for attack of an unsaturated radical by NO₂ to form NO, acrolein, and a normal radical (methyl, ethyl, etc.). These last two reactions share in common that they have not been examined in detail to determine whether they are more appropriately modeled in a two-step process or need to be evaluated utilizing master equation methods as part of a full potential energy surface.

It is important to restate that despite referring to the constructed mechanism as the "v.0" mechanism, it is in fact a newly-constructed mechanism with rates which have already been adjusted based on iterative model predictions and sensitivity analyses to offer generally good agreement to the data.

4.2 Automated mechanism optimization

Owing to the strong non-linearity of the optimization problem, further optimization of the mechanism was carried out utilizing the automated approach of Methling *et al.*⁵⁹. Reaction rates derived from a common analogy were lumped and not optimized independently in order to maintain a physical relation through the optimizer and not arrive at a purely mathematical outcome. Reaction rates of the v.0 mechanism were perturbed by a factor of two at three distinct temperatures, namely 650 K, 825 K, and 1000 K, and updated reaction rate parameters calculated after each iteration of the optimization routine.

Both brute force sensitivity analysis and optimization were per-

formed on the perturbation factors at each of the three temperatures, which were limited to a factor two in the course of this paper. This approach achieves a linearization of the optimization problem, while approximately maintaining a maximum deviation from the original reaction rate due to the maximum alteration factors. The actual optimization minimized the sum of the squared logarithmic errors for a subset of ignition delay times using gradient descent. Experiments in the subset were chosen as every fourth experiment in the complete set. A fixed relaxation factor of 0.6 on the optimizer's step size was implemented in order to prevent divergence or oscillation of the solution. The resulting optimized mechanism is identified here as "version one" or v.1. Sensitivity analysis, simulation, and optimization was implemented utilizing the Python interface of CANTERA.

On the basis of the sensitivity analysis and the model predictions, several classes of reactions were selected for automated optimization to fine-tune their parameters utilizing the method of Methling *et al.*⁵⁹:

- "NO_x-cycling" reactions of the form RO₂ + NO ⇌ RO + NO₂
- Radical recombination to form ROONO in competition with "NO_x-cycling" reactions
- Hydrogen abstractions from *n*-butane and *n*-pentane by NO₂
- Hydrogen abstractions from *n*-alkanes (except methane) by NO
- Nitrite formation from an *n*-alkyl radical and NO₂ (methyl through butyl)

The reactions NO + OH ⇌ HONO, NO + OH ⇌ HNO₂, and H + NO₂ ⇌ NO + OH are not considered for adjustment or optimization as these were recently calculated with high-level theory by Chen *et al.*¹⁴.

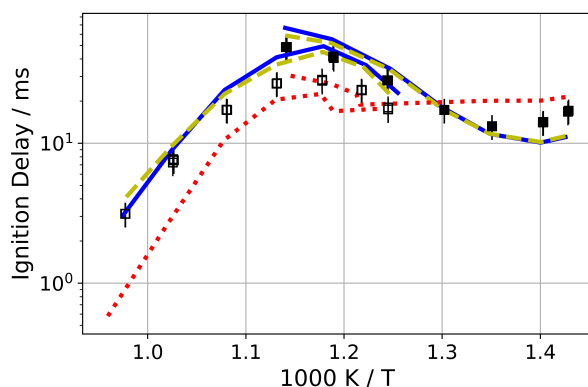


Fig. 7 Model predictions for *n*-pentane in synthetic air diluted with N₂ or Ar at equivalence ratio of $\phi = 1.0$ and with 333 ppm NO₂. Closed symbols (■) are experiments conducted with N₂ diluent; open (□) symbols are Ar diluent. The solid blue line (—) is the v.0 model presented in this work and the dashed yellow line (---) is the optimized v.1 model with improved rate rules. The red dotted line (· · ·) is the model of Marrodán *et al.*

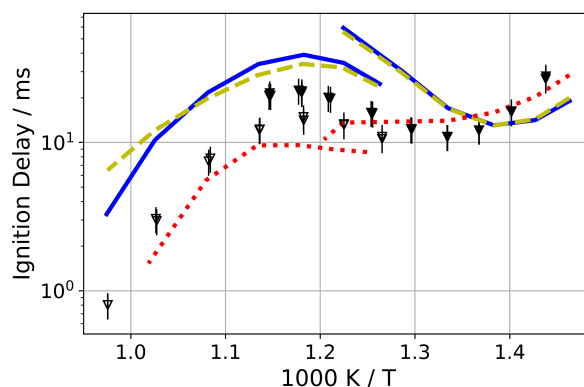


Fig. 8 Model predictions for *n*-pentane in synthetic air diluted with N₂ or Ar at equivalence ratio of $\phi = 1.0$ and initially doped with 1000 ppm NO, fully reacted with O₂ to NO₂ by the start of the experiment. Closed symbols (▼) are experiments conducted with N₂ diluent; open symbols (▽) are Ar diluent. The solid blue line (—) is the v.0 model presented in this work and the dashed yellow line (---) is the optimized v.1 model with improved rate rules. The red dotted line (· · ·) is the model of Marrodán *et al.*

We do include the reactions $C_5H_{12} + NO_2 \rightleftharpoons \text{pentyl} + HONO$ or HNO_2 as these reactions are derived by analogy from the calculations of Chai and Goldsmith²⁷. Further, the reactions involving *n*-butane in lieu of *n*-pentane are also included, despite having been published by Chai and Goldsmith as these rates have not been refit and republished in the exothermic direction, leaving them more susceptible to influence from errors in thermodynamic data. As an aside, the issue of fitting rate in the exothermic direction to minimize errors is discussed in Fuller and Goldsmith¹⁸.

As an extension of including the rates of hydrogen abstraction by NO₂ from alkanes, we also optimize the hydrogen abstractions by NO from ethane to pentane as these have not been previously studied in detail and are fairly uncertain.

Finally, rates for pentyl + NO₂ to form pentyloxy and NO are not included in the optimization as the system for 2-pentyl was examined and extended by analogy to 1-pentyl and 3-pentyl as part of this work. Like the "NO_x-cycling" reactions, a future computational study is planned on R + NO₂ chemistry.

A comparison of the experimental data and predictions of the original and optimized mechanisms alongside those of the mechanism of Marrodán *et al.* for $\phi = 1.0$ is shown in figures 7 and 8. Additional figures for the cases of $\phi = 0.5$ and $\phi = 2.0$ are available in the supplemental materials.

Examining the predictions in figures 7 and 8, we observe that the model presented here, both prior to and post optimization, captures the qualitative curvature of the data well, suggesting that mechanistic aspects of the NTC behaviour are reflected in the model. In the case of the experiments utilizing 333 ppm NO₂ as the dopant (figure 7), agreement the the data are quite good. There is a slight over-prediction of reactivity in the low-temperature branch and under-prediction in the NTC region, but an overall improvement with respect to the model of Marrodán *et al.* in terms of predicted IDTs and the shape of the NTC region curve. For experiments conducted with 1000 ppm as the mixture dopant (figure 8), we see again good qualitative capture of the

NTC curvature but a generally overpredicted ignition delay time at medium and high temperature while overpredicting reactivity at the lowest temperatures.

Bearing those uncertainties in mind, the results of the optimization routine as applied to sensitive and uncertain classes of reactions offer some additional insight. Overall, the improvement made to the predictive capabilities of the mechanism via use of the optimization routine is fairly small, in some cases worsened the predictions. One should bear in mind that the routine was applied in a limited fashion (maximum factor of two adjustment) to a mechanism which has already seen significant adjustment and manual intervention. With a more mature integration of the optimization routine into the modeling and data analysis workflow, we might expect greater value and time savings, particularly as used to attack coupled sensitivities and reaction classes. Proceeding to figures 9, 11, and 12, the estimated rates and optimized rates are compared in the range of experimental temperatures, 650 K to 1000 K. None of these rates are presently modeled as having pressure-dependence.

Examining first the "NO_x-cycling" reactions, figure 9, results suggest further increase in the cycling rates for those involving propyl through pentyl at the primary radical site. The secondary radical site, however, shows a different fit with the rate increased at the lowest temperatures and decreased at the highest. These reactions are expected to actually have pressure-dependence and compete with radical recombinations to form collisionally-stabilized unimolecular products, in this case ROONO. The rate optimization for the stabilization of the "NO_x-cycling" reactants and products to unimolecular wells from both directions is provided in figure 10. Optimization suggests that these rates should also be further increased, indicating that the interconversion between NO and NO₂ is currently under-estimated. The high uncertainty associated with the estimates for these reactions and their relative importance to predictions of IDT, particularly in the NTC

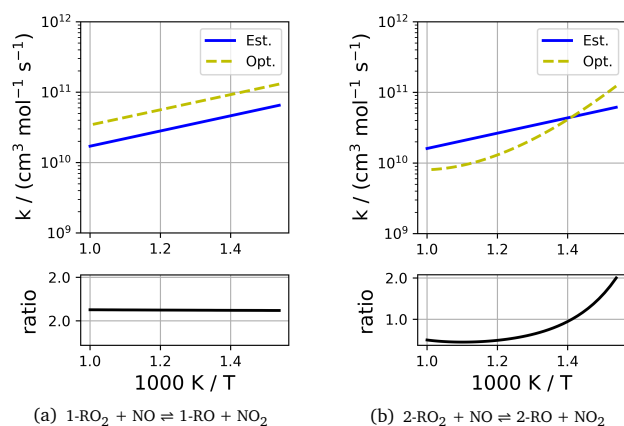


Fig. 9 Comparison of estimated and optimized rates for NO_x -cycling reactions of the form $\text{RO}_2 + \text{NO} \rightleftharpoons \text{RO} + \text{NO}_2$.

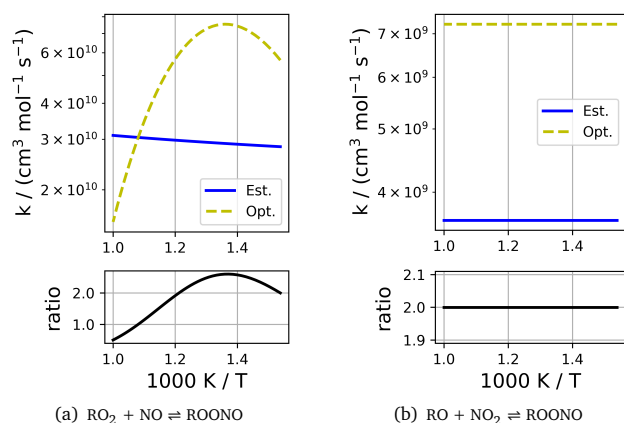


Fig. 10 Comparison of estimated and optimized rates for unimolecular product formation in competition with NO_x -cycling.

region, will hopefully motivate further high-level theoretical studies of the pressure-dependent behaviour.

Examining next hydrogen abstractions from alkanes by NO_x , all rates for NO_2 show the same behaviour: At the highest and lowest temperatures, the rates are essentially unchanged, while at the midpoint (850 K), the rate has been increased by a factor of two. Plots of all ten rates for hydrogen abstractions by NO_2 are found in the supplemental materials. When the abstraction is by NO , figure 11, the results are more mixed

Finally, for optimization of nitrite formation from an alkyl radical and NO_2 , there again appears to be no consistent trend. Throughout the optimization process, there are a number of "bell"-shaped fits which are achieved which provide enhanced model performance, but do not conform to theoretical expectations of reaction rates, particularly for elementary reactions.

These results point to the a fundamental flaw of the general scheme of "postdictive"⁶⁰ of model fitting, where the complexity and coupling of the chemical system make direct measurement or inference of the relevant pathways and rates extremely difficult.

Improvements to the modeling of this and other systems containing novel chemistry ultimately demand both significantly

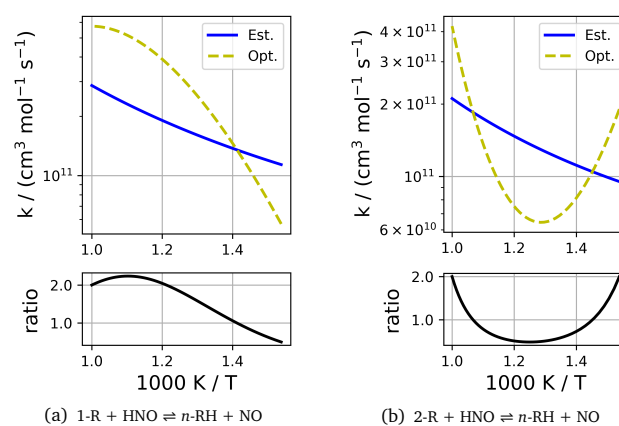


Fig. 11 Comparison of estimated and optimized rates for hydrogen abstraction reactions of the form $\text{RH} + \text{NO} \rightleftharpoons \text{R} + \text{HNO}$.

more and varied experimental data for validation and fundamentally different approaches to mechanism construction. The current manual construction of a mechanism may be replaced with automated construction utilizing databases of known reaction families, but significantly greater gains should be possible by including theoretical and computational methods within the automated mechanism development. Future development of the mechanism for this chemical system is intended to be performed utilizing *ab initio* methods and increased application of theoretical calculations in conjunction with existing mechanisms and experimental data, such as automated potential energy surface explorations⁶¹, automated rates calculations⁶², or automated mechanism generation^{37,38}.

4.3 JSR

To this point, mechanism development and performance has been discussed in terms of the RCM ignition delay data collected and discussed in this present work. Utilizing the data provided by Marrodán *et al.*, the mechanisms may be compared for neat pentane oxidation (figure 13), with 400 ppm of NO_2 (figure 14), and with 1000 ppm of NO (figure 15).

For the neat pentane experiments conducted in the JSR, the addition of nitrogen chemistry and its optimization have no impact on the predictions in the current work: the Bugler *et al.* mechanism and the present work, with and without optimization, show identical results and these closely track those of the Marrodán *et al.* model (see figure 13).

Examining first JSR experiments with NO_2 , the mechanisms all show similar trends with minor differences in peak values and onset points, but are qualitatively similar in predictive capability. Between 600 and 650 K, the greatest differences are observed where the present work and Marrodán *et al.* straddle the data for NO_2 and $\text{HONO} + \text{HNO}_2$ concentrations: the present work under-predicts both, while the model of Marrodán *et al.* over-predicts both. This likely indicates that the overall rate of formation of nitrogenated compounds such as nitrites and nitrates is over-predicted in the present work in this narrow temperature range, but was virtually absent in the mechanism of Marrodán *et al.*

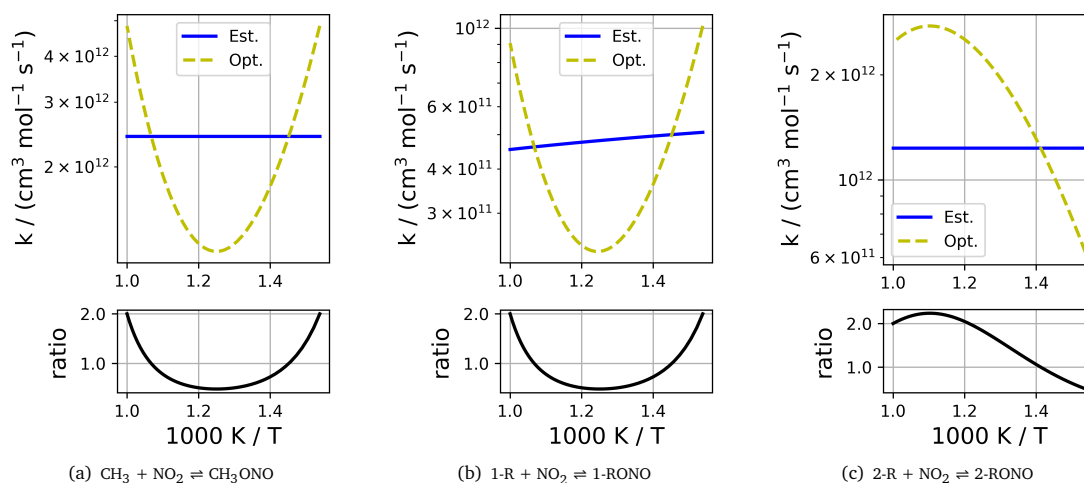


Fig. 12 Comparison of estimated and optimized rates for reactions of the form $R + NO_2 \rightleftharpoons RONO$.

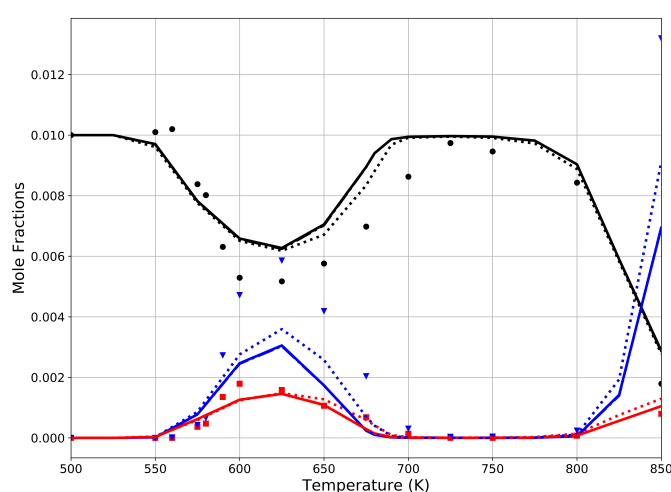


Fig. 13 Comparison of mechanisms for neat pentane oxidation in JSR: points are experimental measurements and lines are simulation results. Black circles and lines for n-pentane (●), red squares and lines for CH_2O (■), and blue triangles and lines for CO (▼). Solid lines (—) are the v.0 model presented in this work. The optimized v.1 model with improved rate rules is identified with dashed lines (---, obscured by the v.0 model results). Dotted lines (.....) are the model of Marrodán *et al.*

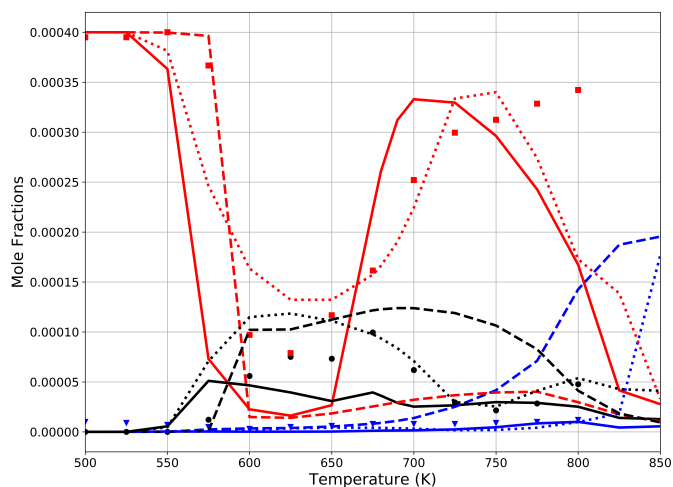


Fig. 14 Comparison of mechanisms for pentane oxidation with 400 ppm NO_2 in JSR: points are experimental measurements and lines are simulation results. Black circles and lines for $HONO + HNO_2$ (●), red squares and lines for NO_2 (■), and blue triangles and lines for NO (▼). Solid lines (—) are the v.0 model presented in this work. The optimized v.1 model with improved rate rules is identified with dashed lines (---, obscured by the v.0 model results). Dotted lines (.....) are the model of Marrodán *et al.*

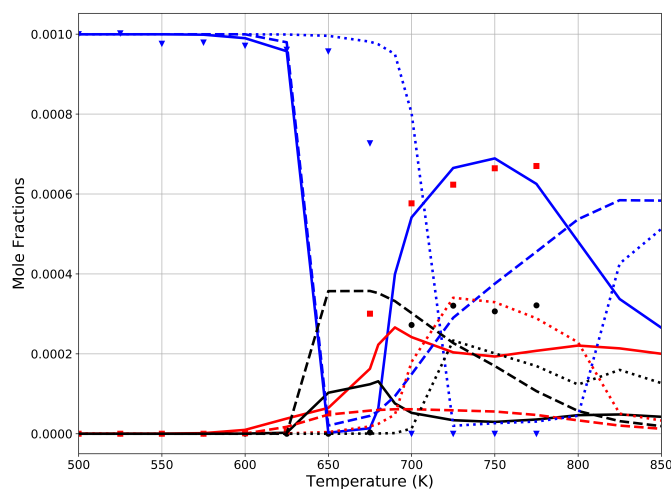


Fig. 15 Comparison of mechanisms for pentane oxidation with 1000 ppm NO in JSR: points are experimental measurements and lines are simulation results. Black circles and lines for HONO + HNO₂ (●), red squares and lines for NO₂ (■), and blue triangles and lines for NO (▼). Solid lines (—) are the v.0 model presented in this work. The optimized v.1 model with improved rate rules is identified with dashed lines (---, obscured by the v.0 model results). Dotted lines (.....) are the model of Marrodán *et al.*

et al., as described in the model development in section 3.

Turning to the JSR experiments with NO as the dopant, we observe first that the onset of conversion of NO to NO₂ starts around 50 K later than the experimental data in Marrodán *et al.*, but occurs far too rapidly in the v.0 mechanism of the present work. Having identified the OOQOOH + NO reactions present in the model of Marrodán *et al.* as problematic, we examine their impact in modeling of the JSR data: Both addition of the OOQOOH + NO reactions to the v.0 mechanism or optimization resulting in the v.1 mechanism (no OOQOOH + NO reactions) lead to similar improvements in the onset of conversion, *i.e.* it is possible to eliminate the OOQOOH + NO reactions and still achieve similar model fidelity. The effect of the OOQOOH + NO reactions on the JSR modeling may be captured with mechanism optimization and adjustments to other rates within a factor of two. Temperature-shifting the onset of NO consumption thus appears to be a function of adjusting the branching between fuel involved in low-temperature combustion processes (first, second oxygen addition) and reactions with NO.

All of the mechanisms under consideration, however, do not capture the depletion of NO and "permanent" conversion to NO₂. The v.0 and Marrodán *et al.* mechanisms do both predict zero NO concentration, but then a rebound. This rebound in NO concentration in the mechanism of Marrodán *et al.* appears to be the fault of NO_x-cycling rates which are much too fast and lead to the large over-predictions in IDT at low temperatures. The v.1 optimized mechanism and the v.0 with OOQOOH + NO reactions show an NO profile which tracks the NO₂ concentration from about 700 K. Concentrations of NO₂ and HONO + HNO₂ are under-predicted by all mechanisms. The onset temperature of NO₂ is formation correct in the present work, but too high in Marrodán *et al.* For HONO + HNO₂, the formation onset is strad-

dled with Marrodán *et al.* also predicting too high a temperature, but the present work predicting too low an onset.

Further, all of the mechanisms considered under-estimate the amount of conversion of NO to NO₂ and the quantity of HONO. Significant further investigation, both theoretical and experimental, is required to fully tease out the complex interactions of NO_x and pentane in the low and intermediate temperature regimes. Reactions of the form OOQOOH + NO ⇌ OH + 2CH₂O + C₃H₆ + NO₂, which we have eliminated, might be replaced with elementary reactions in future development. An initial modeling by analogy to NO_x-cycling reactions of the form RO₂ + NO ⇌ RO + NO₂ follows with the substitution of QOOH for R, but leads to OQOOH as the analog of RO, which is structurally generally omitted in systematically-constructed low-temperature hydrocarbon combustion mechanisms *cf.* Curran *et al.*⁶³ and Bugler *et al.*¹⁵. Addition of bimolecular reactions involving OQOOH and unimolecular dissociations thereof would also then be required to close the additional pathways to species currently included in the mechanism without the introduction of non-elementary reactions.

5 Conclusion

Experimental data for RCM IDTs of *n*-pentane doped with NO_x are presented at 15 bar pressure in temperatures in the NTC region. Model results demonstrate that modeling of the effect of NO₂ addition is more mature than for NO. Further, sensitivity analysis and examination of the results of automated mechanism optimization show how critical NO_x-cycling reactions, particularly those of the form RO₂ + NO ⇌ RO + NO₂, are to these experiments in low and intermediate-temperature combustion. The new mechanism presented here is able to provide qualitatively similar agreement to the JSR data of Marrodán *et al.* as the model presented in that work shows improved behaviour in the NTC region for IDTs. Empirical findings from sensitivity analysis and manual fitting also suggest that some of the estimates for interactions of radicals with NO_x taken from RMG estimates and atmospheric chemistry require revision to determine appropriate unified rates across orders of magnitude in pressure and the broad range of temperatures relevant to combustion modeling. Finally, the systematic inclusion and optimization of classes of nitrogen combustion reactions creates a template for the development of expanded and refined nitrogen-combustion chemistry. Future work utilizing this dataset will focus on developing a more comprehensive understanding of the role played by NO_x interactions in the combustion process, particularly in the NTC region and at higher temperatures for NO, with increased utilization of theoretical and *ab initio* methods.

Author Contributions

Data curation, formal analysis (lead), investigation, methodology (supporting), software (lead), visualization, writing - original draft (lead), and writing - review & editing are credited to MEF. Methodology (supporting), software (supporting), and writing - original draft (supporting) are credited to PM. Data analysis (supporting) and verification are credited to MP. Formal analysis (supporting), methodology (supporting), software (supporting),

and writing - original draft (supporting) are credited to CFG. Conceptualization, funding acquisition, methodology (lead), project administration, resources, and supervision are credited to KAH.

Conflicts of interest

There are no conflicts to declare.

Acknowledgments

This project has been funded by DFG, Project ID HE7599/3-1. Simulations were performed with computing resources granted by RWTH Aachen University under project rwth0453. CFG acknowledges support from the U.S. National Science Foundation through Award Number CBET-1553366. MEF thanks Christian Schulz and Rene Büttgen for cooperation and data-sharing with NO-LIF measurements.

References

- 1 J. A. Miller and C. T. Bowman, *Progress in Energy and Combustion Science*, 1989, **15**, 287–338.
- 2 A. M. Dean and J. W. Bozzelli, in *Combustion Chemistry of Nitrogen*, Springer New York, New York, NY, 2000, ch. 2, p. 125–341.
- 3 P. Glarborg, J. A. Miller, B. Ruscic and S. J. Klippenstein, *Progress in Energy and Combustion Science*, 2018, **67**, 31–68.
- 4 L. Marrodán, Y. Song, M. L. Lavadera, O. Herbinet, M. de Joannon, Y. Ju, M. U. Alzueta and F. Battin-Leclerc, *Energy & Fuels*, 2019, **33**, 5655–5663.
- 5 M. E. Fuller and C. F. Goldsmith, *The Journal of Physical Chemistry A*, 2019, **123**, 5866–5876.
- 6 G. T. Kalghatgi, *International Journal of Engine Research*, 2014, **15**, 383–398.
- 7 M. E. Fuller, A. Mousse-Rayaleh, C. F. Goldsmith and N. Chaumeix, *Combustion and Flame*, 2021.
- 8 M. D. Le, M. Matrat, A. B. Amara, F. Foucher, B. Moreau, Y. Yu and P.-A. Glaude, *Combustion and Flame*, 2020, **222**, 36–47.
- 9 M. Hartmann, K. Tian, C. Hofrath, M. Fikri, A. Schubert, R. Schießl, R. Starke, B. Atakan, C. Schulz, U. Maas, F. K. Jäger and K. Kühling, *Proceedings of the Combustion Institute*, 2009, **32**, 197–204.
- 10 J. Giménez-López, M. Alzueta, C. Rasmussen, P. Marshall and P. Glarborg, *Proceedings of the Combustion Institute*, 2011, **33**, 449–457.
- 11 A. B. Dempsey, N. R. Walker and R. D. Reitz, *SAE International Journal of Fuels and Lubrication*, 2013, **6**, 170–187.
- 12 D. A. Splitter and R. D. Reitz, *Fuel*, 2014, **118**, 163–175.
- 13 A. M. Ickes, S. V. Bohac and D. N. Assanis, *Energy & Fuels*, 2009, **23**, 4943–4948.
- 14 X. Chen, M. E. Fuller and C. F. Goldsmith, *Reaction Chemistry & Engineering*, 2019, **4**, 323–333.
- 15 J. Bugler, B. Marks, O. Mathieu, R. Archuleta, A. Camou, C. Grégoire, K. A. Heufer, E. L. Petersen and H. J. Curran, *Combustion and Flame*, 2016, **163**, 138–156.
- 16 H. Zhao, A. G. Dana, Z. Zhang, W. H. Green and Y. Ju, *Energy*, 2018, **165**, 727–738.
- 17 H. Zhao, L. Wu, C. Patrick, Z. Zhang, Y. Rezgui, X. Yang, G. Wysocki and Y. Ju, *Combustion and Flame*, 2018, **197**, 78–87.
- 18 M. E. Fuller and C. F. Goldsmith, *Proceedings of the Combustion Institute*, 2019, **37**, 695–702.
- 19 P. Dagaut, P. Glarborg and M. Alzueta, *Progress in Energy and Combustion Science*, 2008, **34**, 1–46.
- 20 A. Konnov, *Combustion and Flame*, 2009, **156**, 2093–2105.
- 21 M. Abian, M. U. Alzueta and P. Glarborg, *International Journal of Chemical Kinetics*, 2015, **47**, 518–532.
- 22 S. F. Ahmed, J. Santner, F. L. Dryer, B. Padak and T. I. Farouk, *Energy & Fuels*, 2016, **30**, 7691–7703.
- 23 J. Gimenez-Lopez, C. T. Rasmussen, H. Hashemi, M. U. Alzueta, Y. Gao, P. Marshall, C. F. Goldsmith and P. Glarborg, *International Journal of Chemical Kinetics*, 2016, **48**, 724–738.
- 24 O. Mathieu, J. M. Pemelton, G. Bourque and E. L. Petersen, *Combustion and Flame*, 2015, **162**, 3053–3070.
- 25 O. Mathieu, B. Giri, A. Agard, T. Adams, J. Mertens and E. Petersen, *Fuel*, 2016, **182**, 597–612.
- 26 Y. Zhang, O. Mathieu, E. L. Petersen, G. Bourque and H. J. Curran, *Combustion and Flame*, 2017, **182**, 122–141.
- 27 J. Chai and C. F. Goldsmith, *Proceedings of the Combustion Institute*, 2017, **36**, 617–626.
- 28 A. D. Danilack and C. F. Goldsmith, *Proceedings of the Combustion Institute*, 2018, **1**, 687–694.
- 29 C. Lee, S. Vranckx, K. A. Heufer, S. V. Khomik, Y. Uygun, H. Olivier and R. X. Fernandez, *Zeitschrift für Physikalische Chemie*, 2012, **226**, 1–28.
- 30 C.-J. Sung and H. J. Curran, *Progress in Energy and Combustion Science*, 2014, **44**, 1–18.
- 31 B. Ruscic and D. H. Bross, *Active Thermochemical Tables (ATcT) values based on ver. 1.122g of the Thermochemical Network (2019)*, <https://atct.anl.gov/>.
- 32 B. Ruscic, R. E. Pinzon, M. L. Morton, G. von Laszewski, S. J. Bittner, S. G. Nijssure, K. A. Amin, M. Minkoff and A. F. Wagner, *The Journal of Physical Chemistry A*, 2004, **108**, 9979–9997.
- 33 B. Ruscic, R. E. Pinzon, G. von Laszewski, D. Kodeboyina, A. Burcat, D. Leahy, D. Montoy and A. F. Wagner, *Journal of Physics: Conference Series*, 2005, **16**, 561–570.
- 34 D. G. Goodwin, R. L. Speth, H. K. Moffat and B. W. Weber, *Cantera: An Object-oriented Software Toolkit for Chemical Kinetics, Thermodynamics, and Transport Processes*, <https://www.cantera.org>, 2018, Version 2.4.0.
- 35 C. J. Annesley, J. B. Randazzo, S. J. Klippenstein, L. B. Harding, A. W. Jasper, Y. Georgievskii, B. Ruscic and R. S. Tranter, *The Journal of Physical Chemistry A*, 2015, **119**, 7872–7893.
- 36 J. B. Randazzo, M. E. Fuller, C. F. Goldsmith and R. S. Tranter, *Proceedings of the Combustion Institute*, 2019, **37**, 703–710.
- 37 C. W. Gao, J. W. Allen, W. H. Green and R. H. West, *Computer Physics Communications*, 2016, **203**, 212–225.
- 38 M. Liu, A. G. Dana, M. Johnson, M. Goldman, A. Jocher, A. M. Payne, C. Grambow, K. Han, N. W.-W. Yee, E. Mazeau, K. Blomdal, R. West, F. Goldsmith and W. H. Green, *Journal of Chemical Information and Modeling*, 2021.

- 39 S. W. Benson and J. H. Buss, *The Journal of Chemical Physics*, 1958, **29**, 546–572.
- 40 S. Grimme, *The Journal of Chemical Physics*, 2006, **124**, 034108.
- 41 S. Grimme, J. Antony, S. Ehrlich and H. Krieg, *The Journal of Chemical Physics*, 2010, **132**, 154104.
- 42 L. Goerigk and S. Grimme, *Physical Chemistry Chemical Physics*, 2011, **13**, 6670.
- 43 M. J. Frisch, G. W. Trucks, H. B. Schlegel, G. E. Scuseria, M. A. Robb, J. R. Cheeseman, G. Scalmani, V. Barone, G. A. Petersson, H. Nakatsuji, X. Li, M. Caricato, A. V. Marenich, J. Bloino, B. G. Janesko, R. Gomperts, B. Mennucci, H. P. Hratchian, J. V. Ortiz, A. F. Izmaylov, J. L. Sonnenberg, D. Williams-Young, F. Ding, F. Lipparini, F. Egidi, J. Goings, B. Peng, A. Petrone, T. Henderson, D. Ranasinghe, V. G. Zakrzewski, J. Gao, N. Rega, G. Zheng, W. Liang, M. Hada, M. Ehara, K. Toyota, R. Fukuda, J. Hasegawa, M. Ishida, T. Nakajima, Y. Honda, O. Kitao, H. Nakai, T. Vreven, K. Throssell, J. A. Montgomery, Jr., J. E. Peralta, F. Ogliaro, M. J. Bearpark, J. J. Heyd, E. N. Brothers, K. N. Kudin, V. N. Staroverov, T. A. Keith, R. Kobayashi, J. Normand, K. Raghavachari, A. P. Rendell, J. C. Burant, S. S. Iyengar, J. Tomasi, M. Cossi, J. M. Millam, M. Klene, C. Adamo, R. Cammi, J. W. Ochterski, R. L. Martin, K. Morokuma, O. Farkas, J. B. Foresman and D. J. Fox, *Gaussian 16 Revision C.01*, 2016, Gaussian Inc. Wallingford CT.
- 44 F. Pavošević, C. Peng, P. Pinski, C. Riplinger, F. Neese and E. F. Valeev, *The Journal of Chemical Physics*, 2017, **146**, 174108.
- 45 F. Neese, *Wiley Interdisciplinary Reviews: Computational Molecular Science*, 2011, **2**, 73–78.
- 46 A. Ghysels, T. Verstraelen, K. Hemelsoet, M. Waroquier and V. V. Speybroeck, *Journal of Chemical Information and Modeling*, 2010, **50**, 1736–1750.
- 47 Y. Georgievskii, J. A. Miller, M. P. Burke and S. J. Klippenstein, *The Journal of Physical Chemistry A*, 2013, **117**, 12146–12154.
- 48 Y. Georgievskii and S. J. Klippenstein, MESS: Master Equation System Solver 2016.3.23, <http://tcg.cse.anl.gov/papr/codes/mess.html/>.
- 49 Y. Georgievskii, J. A. Miller, M. P. Burke and S. J. Klippenstein, PAPER: Predictive Automated Phenomenological Rates v1, <http://tcg.cse.anl.gov/papr/>.
- 50 F. L. Nesbitt, W. A. Payne and L. J. Stief, *The Journal of Physical Chemistry*, 1989, **93**, 5158–5161.
- 51 L. Batt, *International Reviews in Physical Chemistry*, 1987, **6**, 53–90.
- 52 M. J. Frost and I. W. M. Smith, *Journal of the Chemical Society, Faraday Transactions*, 1990, **86**, 1751.
- 53 V. Daële, A. Ray, I. Vassalli, G. Poulet and G. L. Bras, *International Journal of Chemical Kinetics*, 1995, **27**, 1121–1133.
- 54 G. D. Mendenhall, D. M. Golden and S. W. Benson, *International Journal of Chemical Kinetics*, 1975, **7**, 725–737.
- 55 M. P. Rissanen, S. L. Arppe, A. J. Eskola, M. M. Tammi and R. S. Timonen, *The Journal of Physical Chemistry A*, 2010, **114**, 4811–4817.
- 56 R. Atkinson, D. L. Baulch, R. A. Cox, J. N. Crowley, R. F. Hampson, R. G. Hynes, M. E. Jenkin, M. J. Rossi, J. Troe and I. Subcommittee, *Atmospheric Chemistry and Physics*, 2006, **6**, 3625–4055.
- 57 M. A. Mueller, R. A. Yetter and F. L. Dryer, *International Journal of Chemical Kinetics*, 2000, **32**, 317–339.
- 58 Z. Chen, P. Zhang, Y. Yang, M. J. Brear, X. He and Z. Wang, *Combustion and Flame*, 2017, **186**, 94–104.
- 59 T. Methling, M. Braun-Unkhoff and U. Riedel, *Combustion Theory and Modelling*, 2016, **21**, 503–528.
- 60 W. H. Green, *AIChE Journal*, 2020, **66**, 1–16.
- 61 R. Van de Vijver and J. Zádor, *Computer Physics Communications*, 2020, **248**, 106947.
- 62 A. Grinberg Dana, D. Ranasinghe, H. Wu, C. Grambow, X. Dong, M. Johnson, M. Goldman, M. Liu and W. Green, *ARC - Automated Rate Calculator; version 1.1.0*, <https://github.com/ReactionMechanismGenerator/ARC>, 2019.
- 63 H. Curran, P. Gaffuri, W. Pitz and C. Westbrook, *Combustion and Flame*, 1998, **114**, 149–177.